Purple nanometrics pigments based on cobalt-doped manganese molybdate: Synthesis, characterization, structural, thermal, optical, colorimetric and chemical properties

Hind Lakhlifi, Youssef El Jabbar, Sophie Guillemet-Fritsch, Bernard Durand, Lahcen Er-Rakho, Rachida El Ouatib

Purple nanometrics pigments based on cobalt-doped manganese molybdate: Synthesis, characterization, structural, thermal, optical, colorimetric and chemical properties.

H. Lakhlifi[a]*, Y. El Jabbar[a], S. Guillemet-Fritsch[b], B. Durand[b], L. Er-Rakho[a], R. El Ouatib[a]

[a] Laboratoire de Physico-chimie des Matériaux Inorganiques, Faculté des sciences Aïn chock, Université Hassan II, Bb. 5366 Mâarif, Casablanca, Morocco

[b] Institut Carnot CIRIMAT, CNRS Université de Toulouse, 118 route de Narbonne, 31062 Toulouse Cedex 9, France.

* Corresponding author email: lakhlifihind21@gmail.com (Hind Lakhlifi)

Abstract

This work is related to the characterization of nanometrics materials of the $\beta MnMoO_4$-$\beta CoMoO_4$ system, prepared by co-precipitation and sol-gel routes from the corresponding metal salts. The structural, morphological and colorimetric characteristics of the obtained powders were studied using thermogravimetric and differential thermal analysis (TGA-DTA), X-ray diffraction (XRD), infrared and Raman spectroscopy, scanning electron microscopy (SEM) and colorimetry (CIE-L*a*b* system). The surface specific area was calculated using the Brunauer–Emmett–Teller analysis (BET) in the adsorption/desorption isotherm. The X-ray diffraction patterns highlighted the formation of a continuous solid solution $Mn_{1-x}Co_xMoO_4$ ($0 \leq x \leq 1$) of monoclinic symmetry (C_2/m) isotype to β-$MnMoO_4$ and this regardless of the synthetic route adopted. FTIR and Raman spectroscopy analysis showed that the chemical bonds' nature in the $Mn_{1-x}Co_xMoO_4$ compounds corresponded to the strong Mo-O-Mo, Mo-O and Co-O-Mo vibrational modes. The micrographs (SEM) highlighted the form of nanorods with sizes ranging from 10 to 200 nm for compositions x=0.3 and x=0.6, prepared by co-precipitation. The specific surface area measurements indicated that the powders obtained by the sol-gel process present lower values than those prepared by co-precipitation, regardless the cobalt substitution rate. The specific surface area of the purple nanoscale powder (x=0.6) obtained by co-precipitation was about 7.52 m^2/g. Colorimetric parameters analysis of the powders heat treated at 1100 °C showed that the degree of the component (-b*) was significant for compositions x=0.6, regardless of the synthesis method adopted.

Keywords: Co-precipitation; Sol-Gel; Nanometrics materials; FTIR; Raman; CIE-L* a* b * system.

1. Introduction

The divalent element molybdates ($AMoO_4$ A= Co^{2+}, Zn^{2+}, Cu^{2+}...) have attracted plenty of attention in recent years because of their thermochromic, piezochromic, and tribochromic applications [1–5]. Indeed, studies on tungsten-doped copper molybdate $CuMo_{1-x}W_xO_4$ have shown that the tungsten content can control the temperature or pressure of the $\alpha \rightarrow \gamma$ phase transition in this molybdate. As these two polymorphic varieties are of different colors (green and ocher, respectively), considering the use of this material as an indicator of temperature or pressure is thus possible [6–9]. Recently, the work carried out in our laboratory by H. Lakhlifi et al. [10–12] showed that the partial substitution of cation A in the matrix of $A_{1-x}Co_xMoO_4$ (A=Zn and Mg) by the chromophoric element cobalt allows the synthesis of new colored materials. Indeed, Co^{2+} ions can induce different colorations depending on the environment they occupy. For example, in the tetrahedral site, they are at the origin of a blue color [10], while in regular octahedral coordination, a pink color is observed, and a purple hue is obtained when the latter is deformed [12].

The $Mn_{1-x}Co_xMoO_4$ composite is likely to be formed, due to the size and electronegativity of the metal (Mn) such as $X_{Mn}<X_{Co}$. The $CoMoO_4$ molybdate is likely to have a more compact structure, leading to the formation of octahedral MoO_6 (α-phase) [13], while the crystal cell, with a higher volume containing tetrahedral MoO_4 (β-phase) [14], is preferred to occur in $MnMoO_4$ [15–17]. However, a transition from α phase to a β phase has been reported experimentally in the $CoMoO_4$ system [18]. Several synthesis methods have been used to synthesize the molybdate $AMoO_4$ (A= Co, Zn, Ni, Cu…) such as the solvothermal method [19], the Pechini method [20], the sol–gel route [21–24], and the solid-solid route [10]. In the present work, we proposed to elaborate on and study molybdates by substituting the manganese in β–$MnMoO_4$ with cobalt. Indeed, with this matrix being beige, its doping by a chromophore element such as cobalt can highlight a piezochromic phenomenon for this material [25]. To evaluate the synthesis method's effect on the molybdates' quality, as well as to compare the results with those obtained in the synthesis by the polymerizable complex route (sol-gel), we opted to elaborate on the solid solutions $Mn_{1-x}Co_xMoO_4$ ($0 \leq x \leq 1$) by co-precipitation. X-ray diffraction, FTIR, Raman spectroscopy, particle size, morphology, surface specific area, colorimetric parameters, and thermal stability were discussed in detail.

2. Methods and materials

2.1. Synthesis

The synthesis by the sol gel route of the solid solution $Mn_{1-x}Co_xMoO_4$ ($0 \leq x \leq 1$) consists of instilling in the solution the salts of divalent cations: manganese nitrate $Mn(NO_3)_2,6H_2O$ (Aldrich,98%), cobalt nitrate $Co(NO_3)_2$, $6H_2O$ (Aldrich,98%) in the presence of ammonium heptamolybdate $(NH4)_6Mo_7O_{24},4H_2O$ (Acros,99%) in a stoichiometric amount. To this mixture, an excess of citric acid (Acros,98%) was added to complex the different cations, with the pH being controlled. We thus obtained a matrix that insured the homogeneous presence of the various cations. The evaporation of the solution at 80°C led to the formation of gels. These gels were dried at 120°C for 24 hours and then calcined at 300°C under air for 12 hours. A heat treatment in the air at an adequate temperature allows for the isolating of powders of different colors.

The synthesis of $Mn_{1-x}Co_xMoO_4$ ($0 \leq x \leq 1$) molybdates by the co-precipitation method consists of making precipitated in aqueous medium in hydrated form. To do this, mixtures of solutions of Mn^{2+} and Co^{2+} cations such that $[Mn^{2+}]+[Co^{2+}]=1$, were added to aqueous solutions of sodium molybdate Na_2MoO_4, under continuous magnetic stirring. Sodium hydroxide solution NaOH (1M) was added dropwise to the mixture to maintain an optimal pH for precipitation. The temperature was fixed at about 80°C. After one hour of stirring, the reaction mixture obtained was washed with distilled water and ethanol several times. This washing allowed to removal of the different residues from the product and to obtain hydrated precursors, as proposed in the following reaction.

$$(1\text{-}x)Mn^{2+} + xCo^{2+} + MnO_4^{2-} + nH_2O \longrightarrow Mn_{1-x}Co_xMoO_4, nH_2O \quad \textbf{(1)}$$

The obtained precursors were dried at 120°C for 12 hours to remove volatile impurities, then ground to fine powders and then calcined in the air for 2 hours, allowing crystallization of the $Mn_{1-x}Co_xMoO_4$ samples.

2.2. Characterization

The decomposition of pre-calcined powders was investigated through differential thermal analysis (DTA) and thermogravimetric analysis (TGA) using a simultaneous DTA/TGA analyzer (DTA-TG-60H Shimadzu). The resulting powders were characterized using an X-ray

diffractometer (Bruker D8 Advance), equipped with a LynxEye detector. The X-ray generator (40kV, 40mA) is a copper anticathode tube that uses the CuKα line. A graphite monochromator eliminates the K_β lines. The wavelength of the $K_{\alpha1}/K_{\alpha2}$ lines of copper is 0.15406 / 0.15443 nm. The phases obtained were analyzed using Eva PLUS software by comparing the positions and intensities of the different diffraction lines observed with those available in the PDF-4-2010 database, established by the ICDD (International Center for Diffraction Data). The infrared spectra were taken using a Fourier-transform infrared spectrometer (IR Affinity-1S Shimadzu). The Raman spectra were recorded with a LabRAM HR 800 (Horiba Jobin-Yvon) spectrometer. The morphologies of the powders were examined using scanning electronic microscopy (JEOL JSM 6400), and the specific surface areas were determined using the Brunauer‑Emmett‑Teller (BET) method (Micrometrics Flowsorb II 2300). The color parameters (L*a*b*) were measured using the CIE Lab system colorimeter (CR-400/410, KONICA MINOLTA).

3. Results and discussion

3.1. Thermal analysis

To determine the optimal calcination temperatures of the $Mn_{1-x}Co_xMoO_4$ molybdate powders, thermogravimetric analyses under air with a temperature rise of 5°C/min were carried out in the temperature range of 25–900°C on the precursors corresponding to the composition of $Mn_{0.4}Co_{0.6}MoO_4$ from each synthesis mode. In the case of the precursor obtained from the sol-gel route, the thermogravimetric analysis showed a global loss of 60% distributed across several steps (Fig.1a):

-A first loss, of about 5% starting around 105°C and was accompanied by a weak endothermic effect that could correspond to the dehydration of the sample.
-A second loss, of about 34%, occurred between 340°C and 550°C accompanied by weak exothermic effects that likely due to the combustion of organic species with the release of carbon monoxide and nitrogen.
-A final loss, of about 21%, was accompanied by a strong exothermic effect observed between 580°C and 620°C. This process probably corresponds to the oxidation of the carbon produced during the combustion of the xerogel and to the crystallization of a solid phase. Beyond 650°C, no phenomena were observed on the thermal analysis curve, which indicated that the decomposition of the precursor was complete. The X-ray diffraction analysis (XRD)

of the residue of TGA showed the crystallization of the solid $Mn_{0.4}Co_{0.6}MoO_4$. Based on this result, we could choose the temperature of 700°C as the optimal temperature for the calcination of xerogels obtained from sol gel synthesis.

In the case of the precursor obtained by co-precipitation, the thermal analysis curve indicated a global mass loss of about 8% (Fig.1b). The successive losses accompanied by endothermic and exothermic effects, recorded between 50°C and 350°C, could correspond to the departure of water and to the beginning of crystallization in the corresponding solid phase. For temperatures above 380°C, no phenomena were recorded on the thermal analysis curve, which meant that the decomposition of the precursor was complete. An XRD analysis of the TGA residue confirmed the crystallization of $Mn_{0.4}Co_{0.6}MoO_4$ molybdate. Following this observation, we could adopt 500°C as the optimal temperature for the calcination of the precursors obtained by Co precipitation.

3. 2. X-ray diffraction

A room temperature XRD analysis was conducted to identify the phases formed after treatment at 500°C and 700°C, respectively, of the precursors from co-precipitation and pyrolysis of the gels. The obtained diffractograms highlight, regardless of the synthesis method used, the formation of a continuous solid partition of nominal formula: $Mn_{1-x}Co_xMoO_4$ ($0 \leq x \leq 1$) of monoclinic symmetry, isotype to β-$MnMoO_4$ (PDF: 01-072-028) and to β-$CoMoO_4$ (PDF: 00-021-0868) (Figs.2 and 3). For compositions ($0 \leq x \leq 0.8$), no transition was observed after grinding. The DRX spectrum of the ground and unground composition x=0.6 serves as an example to illustrate this observation (Fig.3b). This allows us to suggest that the β polymorph could be stabilized by manganese doping.

The Enlarged view of XRD peaks of $Mn_{1-x}Co_xMoO_4$ (x=0, 0.3, 0.6, 1) compounds obtained by co-precipitation are given in Figure 4. All peaks are isotopically indexed to the monoclinic β-$CoMoO_4$ phase (JCPDS 00-021-0868). This confirms the formation of a continuous β-$CoMoO_4$-β-$MnMoO_4$ solid solution.

The calculation of crystallite size using the Scherrer equation from width at mid-height measurements of X-ray diffraction lines made in the angular range 19.6°-30.5°, for $Mn_{1-x}Co_xMoO_4$ ($0 \leq x \leq 1$) molybdates prepared by sol-gel route, is given in Figure 5. We note that the crystallite size decreases significantly upon the insertion of 30% cobalt, beyond the composition x=0.6, stable crystallite sizes ≈ 53 nm are noted.

3.3. Infrared spectroscopy

To confirm the X-ray diffraction results, infrared spectroscopic analyses were performed on the composition (x=0.3 and x=0.6) of the solid solution $Mn_{1-x}Co_xMoO_4$ elaborated by the sol-gel route (Fig.6a) and by the co-precipitation method (Fig.6b). The infrared spectra show a similar appearance regardless of the synthesis mode adopted; the stretching vibration bands of Mo-O-Mo are observed at 887, 830, 893, and 832 cm^{-1} [26–28]. The bands located at 754 and 760 cm^{-1} are characteristic of the tetrahedral [MoO_4] group, and their presence justifies the existence of the tetrahedral coordination of Mo [29,30]. The band located at 856 cm^{-1} is associated with the vibration mode of the Mo-O band [32], those located at 499 and 480 cm^{-1} are specific to the vibrations of Co-O-Mo bands [12,32].

3.4. Raman spectroscopy

The observed vibrational modes are divided into two characteristics, internal modes; which are generated from the oscillation inside the molecular ionic groups with an immobile center of mass, and external modes; which are vibrations of phonons of the lattice due to the movement of cations. To confirm the results obtained previously, Raman spectroscopic analyses were performed on $Mn_{1-x}Co_xMoO_4$ (x=0.3 and x=0.6) powders elaborated by the sol-gel process (Fig.7a) and by co-precipitation (Fig.7b). The high intensity bands observed at 926 and 924 cm^{-1} correspond to the Mo(1)O(2) symmetric stretching vibration (υ_1(Ag)) [30,33]; the bands located at 874 and 872 cm^{-1} are assigned to the Mo(1)O(1) symmetric stretching vibrations [34]. The peaks at 813 and 810 cm^{-1} are assigned to the anti-symmetric stretching υ_3(Ag/C_2h) and υ_3(Eg) vibration modes of the Mo-O-Mo of German entartet (e.g.), respectively [35,36]. The bands observed at 353 and 350 cm^{-1} correspond to the anti-symmetric υ_4(Bg/D_2h) and υ_2(Ag/C_2h) bending modes, respectively [37–39]. Those located at 320 and 318 cm^{-1} correspond to the stretching vibrations of the Mo-O-Co bands [40]. The free rotation mode was observed at 276 cm^{-1} [41].

3.5. Microstructural characterizations

The powders of the $Mn_{1-x}Co_xMoO_4$ molybdates with x=0.3 and x=0.6 obtained via the sol-gel route, and by co-precipitation, were characterized by scanning electron microscopy (SEM).

The SEM micrographs (Fig.8a) show, for the product obtained via the sol-gel route, that powders formed agglomerates consisting of particles of varied morphology with sizes ranging from 1 to 9 μm. The micrograph of the composition x=0.6 (Fig.8b) shows an advanced pre-sintering state, which explains the low values of the specific surface areas determined for these powders.

The powders obtained by co-precipitation present various morphologies. In fact, the powders of compositions x=0 and x=0.3 (Fig.9a and Fig.9c) are formed by particles with a rectangular parallelepiped shape, which come from agglomerated clusters of heterogeneous morphology. The powders of fractions x=0.6 and x=1 (Fig.9b and Fig.9d) are composed by particles in the form of more dispersed nano-rods; the average size of the particles of these powders is less than 200 nm.

Specific surface area measurements were performed on the $Mn_{1-x}Co_xMoO_4$ compositions (x=0.3 and x=0.6) (Table 1). It was noted that the powders obtained by the sol-gel process presented lower specific surface areas than those obtained by co-precipitation, irrespective of the cobalt content. This can be explained by the effects of exposure to high temperature. The particles of the powders obtained by the sol-gel process appeared spherical and individualized. The average sizes of these particles were deduced by the above formula [42]. They were 9571 nm for the x=0.3 composition and 5963 nm for x=0.6, respectively.

$$\boldsymbol{d = \frac{6}{\rho \times S} 10^3} \qquad \textbf{(2)}$$

d: particle sizes (nm).

ρ: theoretical density (cm^3/g) obtained by Rietveld refinement.

S: specific surface area (m^2/g).

3.6. Evaluation of application properties of the synthesized pigments

The colorimetric parameters (L*a*b*) of the $Mn_{1-x}Co_xMoO_4$ $0 \leq x \leq 1$ powder, obtained at 700°C by the sol-gel method and at 500°C by co-precipitation, were measured in the CIE Lab system (Fig.10a and 10b). It was noted that the component (-b*) that characterized the purple color, changed faintly with the cobalt incorporation rate, regardless of the synthesis method used. The different colors obtained are shown in Figure 11.

The degree of bluing of the compounds prepared by the sol-gel route was higher than that obtained from the powders synthesized by co-precipitation. In order to optimize the processing temperature required for the industrial use of a dye pigment, we processed the

samples (x= 0, 0.3, 0.6, and 1) obtained by both synthesis methods, at a temperature of 1100°C (Fig.12). We noted that the parameter (-b*) presented a maximum in the vicinity of the x=0.6 fraction, irrespective of the method of synthesis used. The relatively high value of this parameter might encourage the use of the composition x= 0.6 as a pigment in ceramic staining. This result was compatible with that obtained in the case of the $Mg_{1-x}Co_xMoO_4$ system ($0 \leq x \leq 1$) [12].

The thermal and colorimetric stability of these pigments was studied in order to evaluate their application as ceramic colorants. The thermal stability was verified by differential thermal analysis (DTA) performed between 25°C and 1100°C with a 10°C/min rise. The curves obtained for the compositions $Mn_{0.7}Co_{0.3}MoO_4$ and $Mn_{0.4}Co_{0.6}MoO_4$ synthesized by co-precipitation and the sol-gel processes, are shown in Figure 13. No thermal phenomena were observed which indicated that these pigments had a good thermal stability.

The stability of the color of the $Mn_{0.7}Co_{0.3}MoO_4$ and $Mn_{0.4}Co_{0.6}MoO_4$ compositions treated at 1100°C for two hours, was evaluated by tests of attacks by chemical agents on the pigments in different media (acid (HNO_3) and basic (NaOH)) titrated at 10%. After two hours of attacks a filtration, washing and drying, colorimetric analyses were performed. The values obtained showed that the colorimetric parameters of these compositions remained unchanged (Table 2). This indicated that these pigments had good stability and resistance to an acid-base test.

4. Conclusion

The elaboration of the $Mn_{1-x}Co_xMoO_4$ ($0 \leq x \leq 1$) molybdates by the sol-gel and co-precipitation methods led to powders with distinct microstructural characteristics. The X-ray diffraction result showed the formation of continuous systems of the solid solution $Mn_{1-x}Co_xMoO_4$ isotype at β-$MnMoO_4$, regardless of the adopted synthesis method. The grinding of the powders with compositions $0 \leq x \leq 0.8$ seemed to have no influence on the obtained pure phase. The powders prepared by co-precipitation have an average particle size below 200 nm. These powders also presented larger specific surface areas (6.39 m^2/g and 7.52 m^2/g) than those obtained by the sol-gel process (0.15 m^2/g and 0.22 m^2/g). This was due to the high calcination temperature (700°C) which led to an advanced pre-sintering phenomenon in the case of powders prepared by the sol-gel process. The SEM images confirm these results. An infrared and Raman spectroscopy showed that the cobalt was well inserted into the β-$MnMoO_4$ system regardless of the synthesis method employed. Measurements of the

colorimetric parameters (L*a*b*) of the $Mn_{1-x}Co_xMoO_4$ ($0 \leq x \leq 1$) system, obtained by both synthesis methods, at a temperature of 1100°C, showed that the component (-b*), which characterized the purple color, presented a maximum in the vicinity of the fraction x=0.6. Thermal and colorimetric stability studies of the $Mn_{0.7}Co_{0.3}MoO_4$ and $Mn_{0.4}Co_{0.6}MoO_4$ pigments confirmed that they showed good stability and resistance under temperature and chemical tests.

References

[1] A.M. Huerta-Flores, I. Juárez-Ramírez, L.M. Torres-Martínez, J.E. Carrera-Crespo, T. Gómez-Bustamante, O. Sarabia-Ramos, Synthesis of AMoO4 (A = Ca, Sr, Ba) photocatalysts and their potential application for hydrogen evolution and the degradation of tetracycline in water, J. Photochem. Photobiol. Chem. 356 (2018) 29–37. https://doi.org/10.1016/j.jphotochem.2017.12.029.

[2] L. Jiang, Z. Wang, H. Chen, Y. Chen, P. Chen, Z. Xu, Thermal annealing effects on the luminescence and scintillation properties of CaMoO4 single crystal grown by Bridgman method, J. Alloys Compd. 734 (2018) 179–187. https://doi.org/10.1016/j.jallcom.2017.11.005.

[3] S. Raghunath, R. Balan, Solvent assisted synthesis and characterization of AMoO4 (A = Ca, Sr & Ba) nanomaterials, Mater. Today Proc. (2021). https://doi.org/10.1016/j.matpr.2020.11.374.

[4] L. Wang, X. Wang, L. Zhong, W. Liang, M. Liu, Y. Zhao, X. Lai, J. Bi, D. Gao, Rhombic dodecahedron-like CoMoO4/C composite: A facile construction and excellent electrochemical performances for lithium-ion batteries, Ceram. Int. 46 (2020) 24257–24266. https://doi.org/10.1016/j.ceramint.2020.06.206.

[5] N. Najafvandzadeh, S. López-Moreno, D. Errandonea, P. Pavone, C. Draxl, First-principles study of elastic and thermal properties of scheelite-type molybdates and tungstates, Mater. Today Commun. 24 (2020) 101089. https://doi.org/10.1016/j.mtcomm.2020.101089.

[6] M. Benchikhi, O. El, S. Guillemet-Fritsch, L. Er-Rakho, B. Durand, Investigation of structural transition in molybdates CuMo1-xWxO4 prepared by polymeric precursor method, Process. Appl. Ceram. 11 (2017) 21–26. https://doi.org/10.2298/PAC1701021B.

[7] I. Pudza, A. Kalinko, A. Cintins, A. Kuzmin, Study of the thermochromic phase transition in CuMo1−xWxO4 solid solutions at the W L3-edge by resonant X-ray emission spectroscopy, Acta Mater. 205 (2021) 116581. https://doi.org/10.1016/j.actamat.2020.116581.

[8] A. Jezierski, Electronic and magnetic properties of Cu2MgV2O8 and CuMg2V2O8 – ab initio study, Solid State Commun. 314–315 (2020) 113943. https://doi.org/10.1016/j.ssc.2020.113943.

[9] W. Zhang, J. Yin, F. Min, L. Jia, D. Zhang, Q. Zhang, J. Xie, Cyclic voltammetry analysis of copper electrode performance in Na2WO4 solution and optical property of electrochemical synthesized CuWO4 nanoparticles, J. Alloys Compd. 690 (2017) 221–227. https://doi.org/10.1016/j.jallcom.2016.08.106.

[10] H. Lakhlifi, Y. El Jabbar, R. El Ouatib, L. Er-Rakho, B. Durand, S. Guillemet-Fritsch, Synthesis of molybdates Zn1-xCoxMoO4 ($0 \leq x \leq 1$), by decomposition of the precursors developed by the glycine-nitrate process (GNP), and their characterization, Mater. Sci. Semicond. Process. 114 (2020) 105054. https://doi.org/10.1016/j.mssp.2020.105054.

[11] H. Lakhlifi, M. Benchikhi, R.E. Ouatib, L. Er-Rakho, S. Guillemet-Fritsch, B. Durand, Synthesis and physicochemical characterization of pigments based on molybdenum « ZnO-MoO3: Co2+», (2015) 5.

[12] H. Lakhlifi, Y.E. Jabbar, R.E. Ouatib, L. Er-Rakho, S. Guillemet-Fritsch, B. Durand, Structural, morphological and optical properties of cobalt-substituted MgMoO4 ceramics prepared by pyrolysis of citric acid precursors, Surf. Interfaces. 21 (2020) 100718. https://doi.org/10.1016/j.surfin.2020.100718.

[13] D. Yu, Z. Zhang, Y. Teng, Y. Meng, X. Zhao, X. Liu, Controllable synthesis of cobalt molybdate nanoarrays on nickel foam as the advanced electrodes of alkaline battery-supercapacitor hybrid devices, J. Alloys Compd. 835 (2020) 155244. https://doi.org/10.1016/j.jallcom.2020.155244.

[14] Y. Zhang, W. Han, X. Long, H. Nie, Redispersion effects of citric acid on CoMo/γ-Al2O3 hydrodesulfurization catalysts, Catal. Commun. 82 (2016) 20–23. https://doi.org/10.1016/j.catcom.2016.04.012.

[15] R. Sheng, J. Hu, X. Lu, W. Jia, J. Xie, Y. Cao, Solid-state synthesis and superior electrochemical performance of MnMoO4 nanorods for asymmetric supercapacitor, Ceram. Int. 47 (2021) 16316–16323. https://doi.org/10.1016/j.ceramint.2021.02.211.

[16] J. Xu, Y. Sun, M. Lu, L. Wang, J. Zhang, J. Qian, X. Liu, Fabrication of hierarchical MnMoO4·H2O@MnO2 core-shell nanosheet arrays on nickel foam as an advanced electrode for asymmetric supercapacitors, Chem. Eng. J. 334 (2018) 1466–1476. https://doi.org/10.1016/j.cej.2017.11.085.

[17] R. Thangappan, R. Dhinesh Kumar, R. Jayavel, Synthesis, structural and electrochemical properties of Mn-MoO4/graphene nanocomposite electrode material with improved performance for supercapacitor application, J. Energy Storage. 27 (2020) 101069. https://doi.org/10.1016/j.est.2019.101069.

[18] R.K.S. Costa, S.C. Teles, P.C. de Sousa Filho, A. Dias, K.P.F. Siqueira, Influence of europium doping on the structural phase-transition temperature of β− and α−CoMoO4 polymorphs, Mater. Res. Bull. 118 (2019) 110517. https://doi.org/10.1016/j.materresbull.2019.110517.

[19] Y. Keereeta, T. Thongtem, S. Thongtem, Effect of medium solvent ratios on morphologies and optical properties of α-ZnMoO4, β-ZnMoO4 and ZnMoO4·0.8H2O crystals synthesized by microwave-hydrothermal/solvothermal method, Superlattices Microstruct. 69 (2014) 253–264. https://doi.org/10.1016/j.spmi.2014.02.011.

[20] M. Maczka, K. Hermanowicz, P.E. Tomaszewski, M. Zawadzki, J. Hanuza, Vibrational and luminescence studies of MIIn(MoO4)2 (MI=K, Rb) and MIAl(MoO4)2 (MI=K, Na) molybdates doped with chromium(III) prepared via the Pechini method, Opt. Mater. 31 (2008) 167–175. https://doi.org/10.1016/j.optmat.2008.02.010.

[21] H. Kausar, Y. Khan, A. Ahmad, S.I. Ahmad, S.A.A. Nami, Synthesis and characterization of zirconium(IV) molybdosulphosalicylate, multi-walled carbon nanotubes and polypyrrole based ternary nanocomposites: Adsorption and lead sensing studies, Synth. Met. 274 (2021) 116730. https://doi.org/10.1016/j.synthmet.2021.116730.

[22] W. Zhang, J. Yin, F. Min, L. Jia, D. Zhang, Q. Zhang, J. Xie, Preparation and photoluminescence properties of MMoO4 (M = Cu, Ni, Zn) nano-particles synthesized via electrolysis, J. Mol. Struct. 1127 (2017) 777–783. https://doi.org/10.1016/j.molstruc.2016.08.020.

[23] F. Hcini, S. Hcini, M.M. Almoneef, M.H. Dhaou, M.S. Alshammari, A. Mallah, S. Zemni, N.

Lefi, M.L. Bouazizi, Thermal, microstructural, optical, magnetic and magnetocaloric studies for Ni0.5Mn0.5Cr2O4 chromite spinel prepared using sol-gel method, J. Mol. Struct. 1243 (2021) 130769. https://doi.org/10.1016/j.molstruc.2021.130769.

[24] Ö. Kesmez, Preparation of hybrid nanocomposite coatings via sol-gel method for hydrophobic and self-cleaning properties, J. Mol. Struct. 1205 (2020) 127572. https://doi.org/10.1016/j.molstruc.2019.127572.

[25] S. Prabhu, A. Gowdhaman, S. Harish, M. Navaneetham, R. Ramesh, Synthesis of petal-like CoMoO4/r-GO composites for high performances hybrid supercapacitor, Mater. Lett. 295 (2021) 129821. https://doi.org/10.1016/j.matlet.2021.129821.

[26] O. Rabbani, S. Ghasemi, S.R. Hosseini, Sonochemical assisted synthesis of manganese–nickel molybdate/reduced graphene oxide nanohybrid for energy storage, J. Alloys Compd. 840 (2020) 155665. https://doi.org/10.1016/j.jallcom.2020.155665.

[27] K.K. Purushothaman, M. Cuba, G. Muralidharan, Supercapacitor behavior of α-MnMoO4 nanorods on different electrolytes, Mater. Res. Bull. 47 (2012) 3348–3351. https://doi.org/10.1016/j.materresbull.2012.07.027.

[28] Electroanalysis and Biotelectrochemistry Lab, Department of Chemical Engineering and Biotechnology, National Taipei University of Technology, No.1, Section 3, Chung-Hsiao East Road, Taipei 106, Taiwan R.O.C., S. Musuvadhi Babulal, Synthesis of MnMoO4 Nanorods by a Simple Co-Precipitation Method in Presence of Polyethylene Glycol for Pseudocapacitor Application, Int. J. Electrochem. Sci. (2020) 7053–7063. https://doi.org/10.20964/2020.07.90.

[29] J. Yesuraj, V. Elumalai, M. Bhagavathiachari, A.S. Samuel, E. Elaiyappillai, P.M. Johnson, A facile sonochemical assisted synthesis of α-MnMoO4/PANI nanocomposite electrode for supercapacitor applications, J. Electroanal. Chem. 797 (2017) 78–88. https://doi.org/10.1016/j.jelechem.2017.05.019.

[30] C. Sekar, R.K. Selvan, S.T. Senthilkumar, B. Senthilkumar, C. Sanjeeviraja, Combustion synthesis and characterization of spherical α-MnMoO4 nanoparticles, Powder Technol. 215–216 (2012) 98–103. https://doi.org/10.1016/j.powtec.2011.09.016.

[31] B. Ramulu, S. Chandra Sekhar, G. Nagaraju, J.S. Yu, Rational design and construction of nickel molybdate nanohybrid composite for high-performance supercapattery, Appl. Surf. Sci. 515 (2020) 146023. https://doi.org/10.1016/j.apsusc.2020.146023.

[32] V. Jeseentharani, A. Dayalan, K.S. Nagaraja, Nanocrystalline composites of transition metal molybdate (Ni1–xCoxMoO4; x = 0, 0.3, 0.5, 0.7, 1) synthesized by a co-precipitation method as humidity sensors and their photoluminescence properties, J. Phys. Chem. Solids. 115 (2018) 75–83. https://doi.org/10.1016/j.jpcs.2017.12.008.

[33] G.K. Veerasubramani, K. Krishnamoorthy, R. Sivaprakasam, S.J. Kim, Sonochemical synthesis, characterization, and electrochemical properties of MnMoO4 nanorods for supercapacitor applications, Mater. Chem. Phys. 147 (2014) 836–842. https://doi.org/10.1016/j.matchemphys.2014.06.028.

[34] Y.-P. Gao, K.-J. Huang, C.-X. Zhang, S.-S. Song, X. Wu, High-performance symmetric supercapacitor based on flower-like zinc molybdate, J. Alloys Compd. 731 (2018) 1151–1158. https://doi.org/10.1016/j.jallcom.2017.10.161.

[35] Y. Chen, Y. Li, Z. Hai, Y. Li, S. Kan, J. Chen, X. Chen, S. Zhuiykov, D. Cui, C. Xue, Facile-synthesized NiCo2O4@MnMoO4 with novel and functional structure for superior performance

supercapacitors, Appl. Surf. Sci. 452 (2018) 413–422. https://doi.org/10.1016/j.apsusc.2018.05.026.

[36] Y. Tian, M. Zhou, X. Meng, Y. Miao, D. Zhang, Needle-like CoMoO with multi-modal porosity for pseudocapacitors, Mater. Chem. Phys. 198 (2017) 258–265. https://doi.org/10.1016/j.matchemphys.2017.06.010.

[37] T. Meng, H. Jia, H. Ye, T. Zeng, X. Yang, H. Wang, Y. Zhang, Facile preparation of CoMoO4 nanorods at macroporous carbon hybrid electrocatalyst for non-enzymatic glucose detection, J. Colloid Interface Sci. 560 (2020) 1–10. https://doi.org/10.1016/j.jcis.2019.10.054.

[38] Z. Liu, J. Wang, C. Zhan, J. Yu, Y. Cao, J. Tu, C. Shi, Phosphide-oxide honeycomb-like heterostructure CoP@CoMoO4/CC for enhanced hydrogen evolution reaction in alkaline solution, J. Mater. Sci. Technol. 46 (2020) 177–184. https://doi.org/10.1016/j.jmst.2019.12.013.

[39] T. Yang, H. Zhang, Y. luo, L. Mei, D. Guo, Q. Li, T. Wang, Enhanced electrochemical performance of CoMoO4 nanorods/reduced graphene oxide as anode material for lithium-ion batteries, Electrochimica Acta. 158 (2015) 327–332. https://doi.org/10.1016/j.electacta.2015.01.154.

[40] J.E. Herrera, D.E. Resasco, Loss of single-walled carbon nanotubes selectivity by disruption of the Co–Mo interaction in the catalyst, J. Catal. 221 (2004) 354–364. https://doi.org/10.1016/j.jcat.2003.08.005.

[41] C. Luz-Lima, J.C. Batista, P.T.C. Freire, G.P. de Sousa, F.E.P. dos Santos, J. Mendes Filho, B.C. Viana, G.D. Saraiva, Temperature-dependent Raman spectroscopy studies of phase transformations in the K2WO4 and the MgMoO4 crystals, Vib. Spectrosc. 65 (2013) 58–65. https://doi.org/10.1016/j.vibspec.2012.11.016.

[42] Y. GAO, H. CHANG, Q. WU, H. WANG, Y. PANG, F. LIU, H. ZHU, Y. YUN, Optical properties and magnetic properties of antisite-disordered Ni1–xCoxCr2O4 spinels, Trans. Nonferrous Met. Soc. China. 27 (2017) 863–867. https://doi.org/10.1016/S1003-6326(17)60099-2.

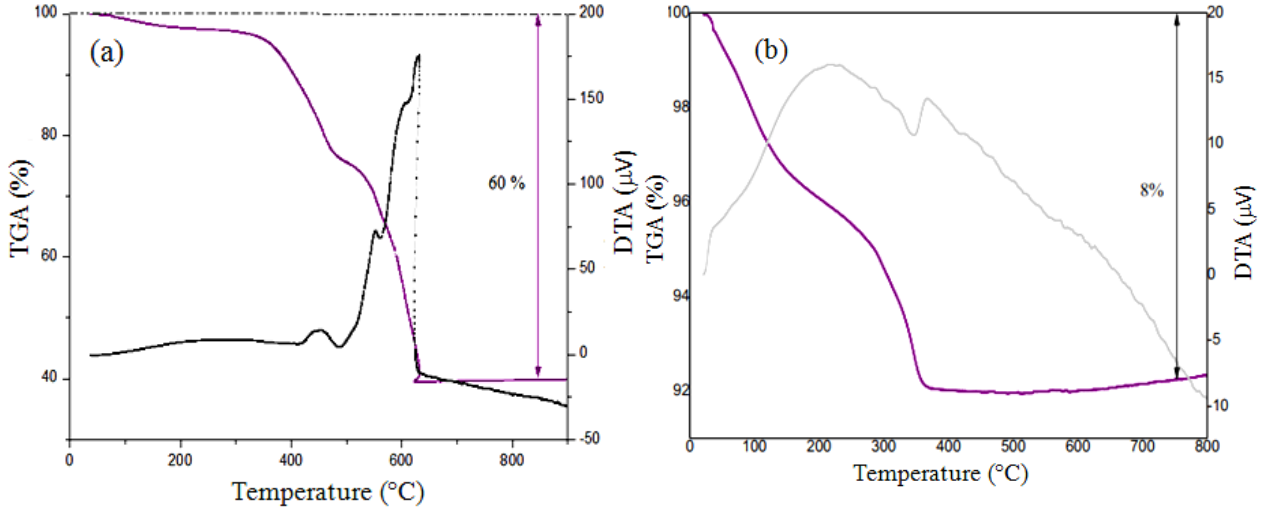

Fig. 1. Thermal analysis (TGA-DTA) curves of $Mn_{0.4}Co_{0.6}MoO_4$ prepared by sol-gel route **(a)** and by co-precipitation **(b)**.

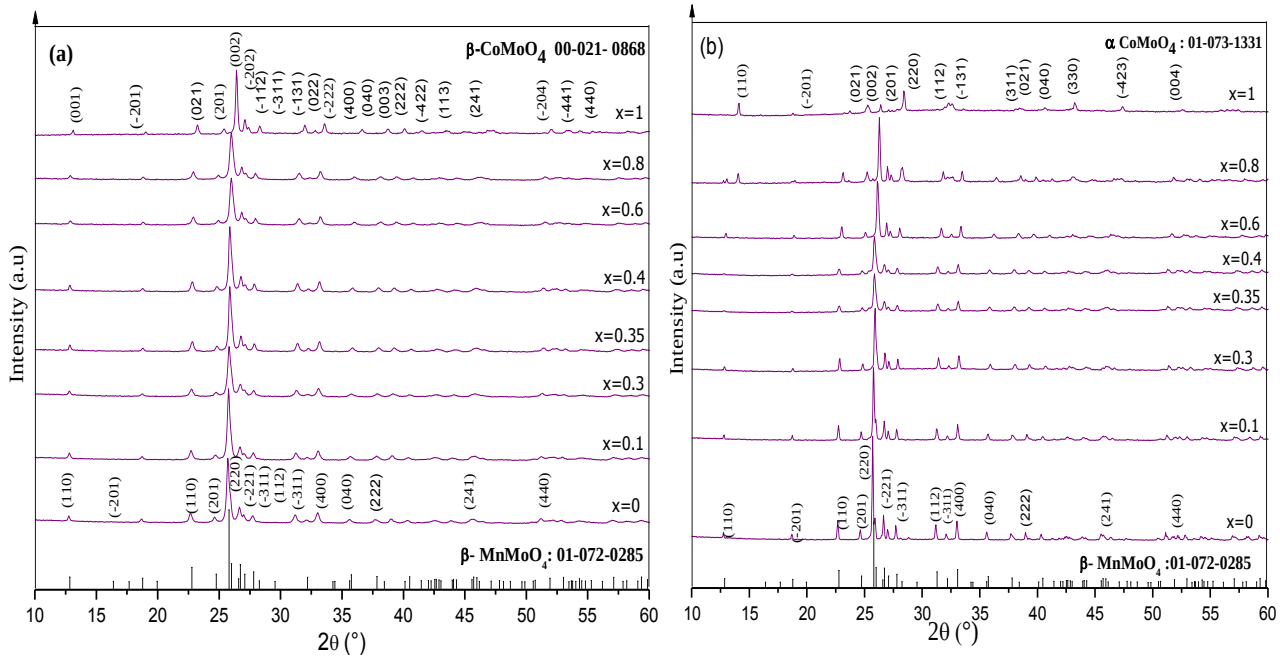

Fig.2. X-ray powder diffraction patterns of $Mn_{1-X}Co_xMoO_4$ ($0 \leq x \leq 1$) prepared by sol-gel at 700°C; **(a)** without grinding and **(b)** with grinding.

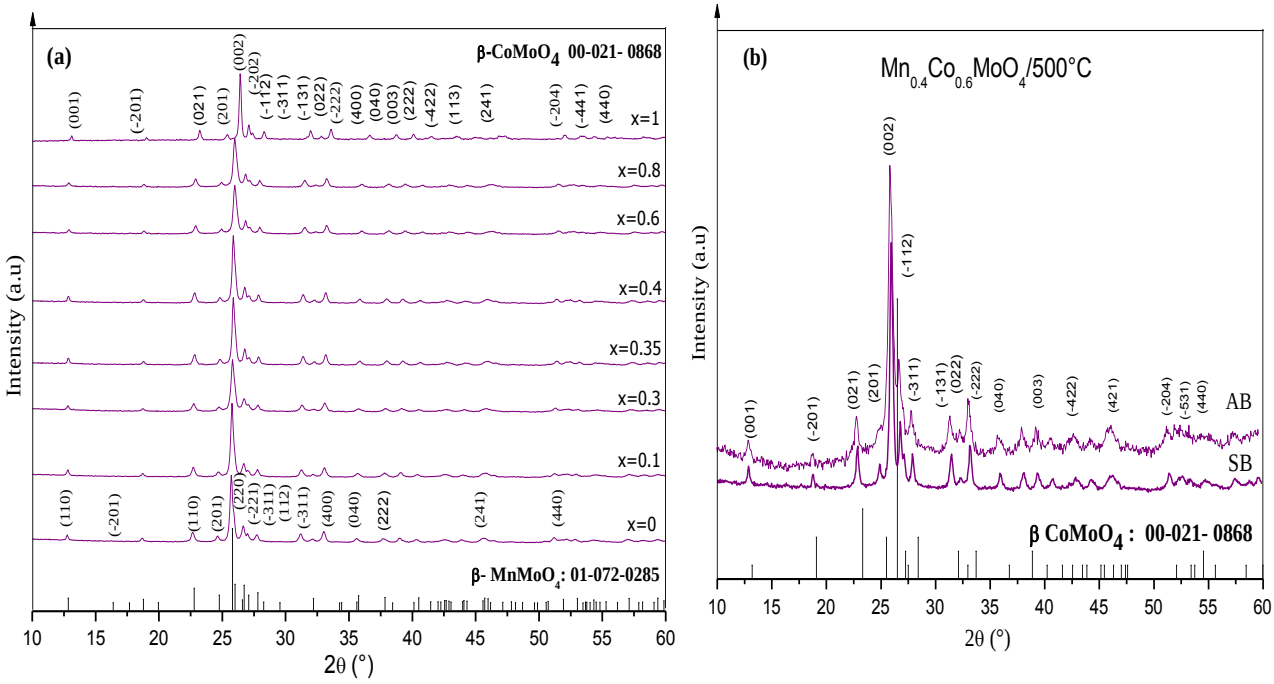

Fig.3. (a) X-ray powder diffraction patterns of $Mn_{1-X}Co_xMoO_4$ ($0 \leq x \leq 1$) prepared by co-precipitation at 500°C and **(b)** X-ray powder diffraction patterns of $Mn_{0.4}Co_{0.6}MoO_4$ (AB : with grinding/SB: without grinding).

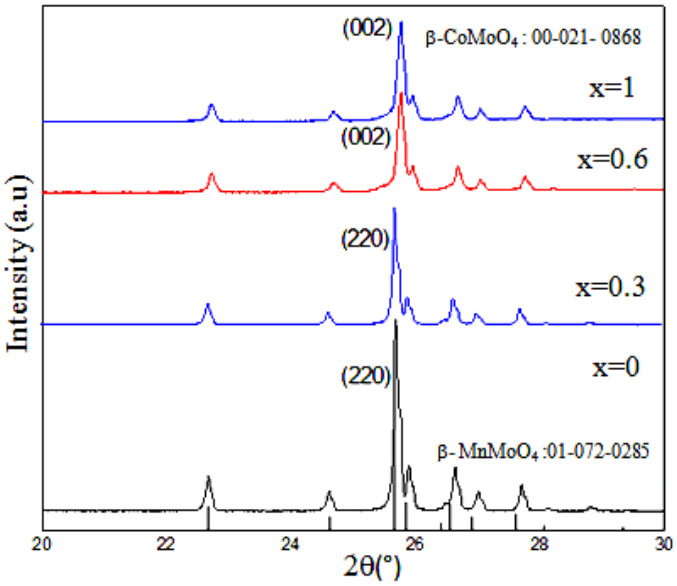

Fig.4. Enlarged view of XRD peaks of $Mn_{1-x}Co_xMoO_4$ (x=0, 0.3, 0.6, 1) compounds in the 2θ range of 20–30°.

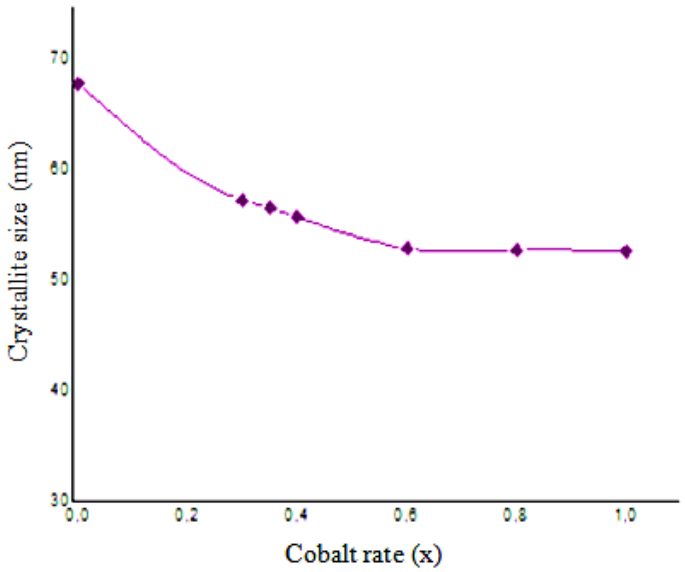

Fig.5. Evolution and growth of crystallite size of $Mn_{1-x}Co_xMoO_4$ compounds prepared by sol gel route, deduced from the Scherrer equation using XRD line broadening, as a function of Co (x) rates $0 \leq x \leq 1$.

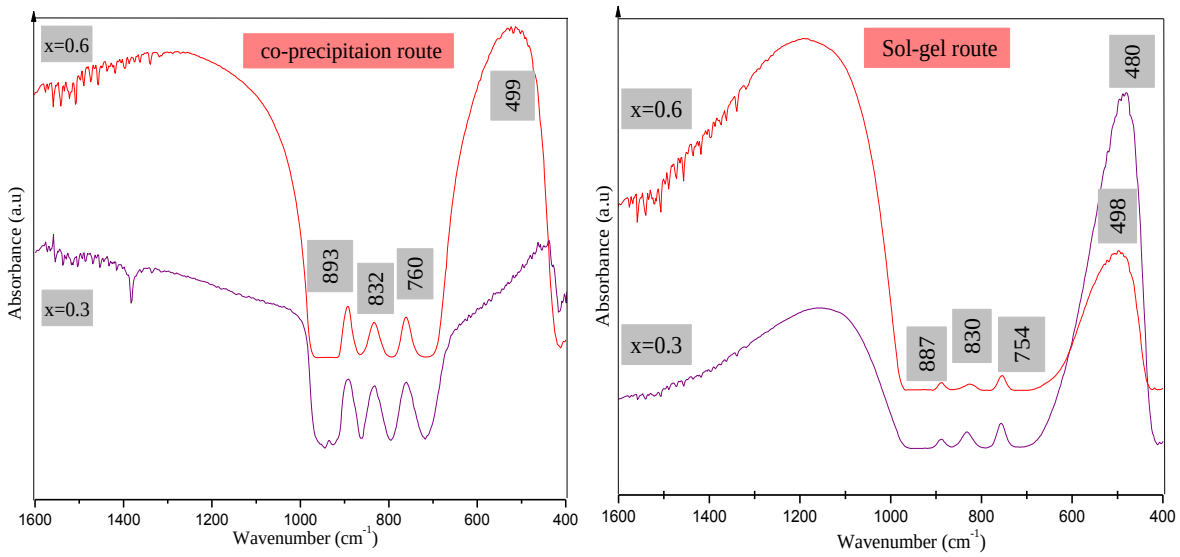

Fig.6. FT-IR spectra of $Mn_{1-x}Co_xMoO_4$ (x=0.3 and x=0.6) powders obtained by sol-gel route and by co-precipitation.

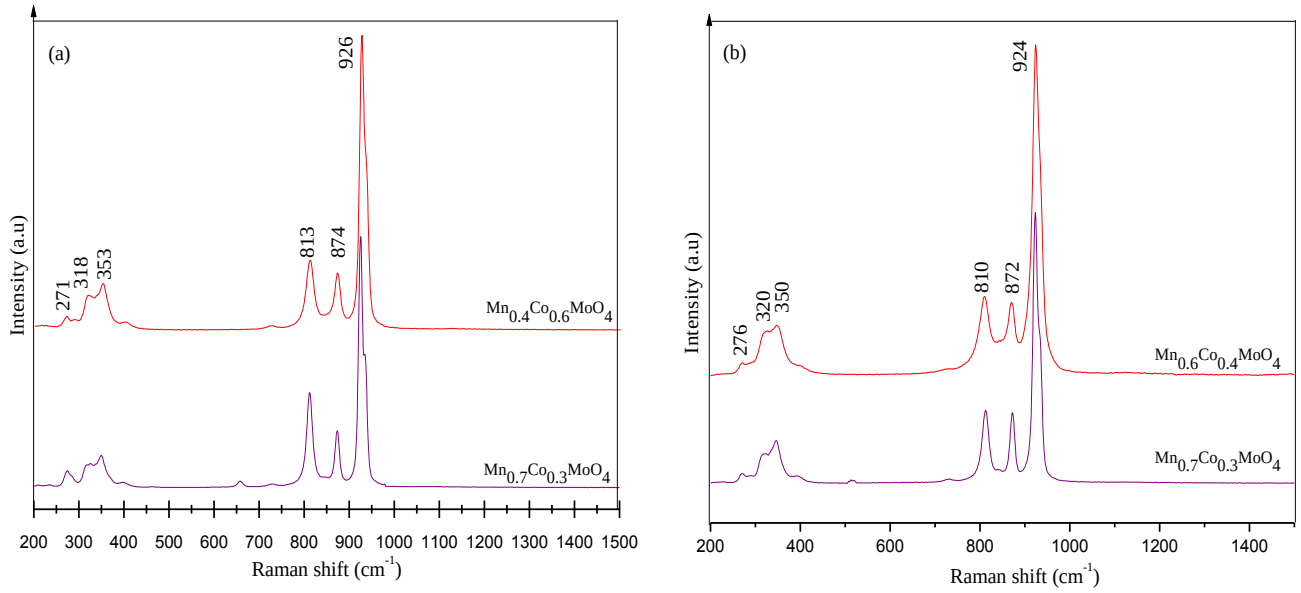

Fig.7. Raman spectra of $Mn_{1-x}Co_xMoO_4$ (x=0.3 and x=0.6) powders prepared by sol-gel (a) and co-precipitation (b).

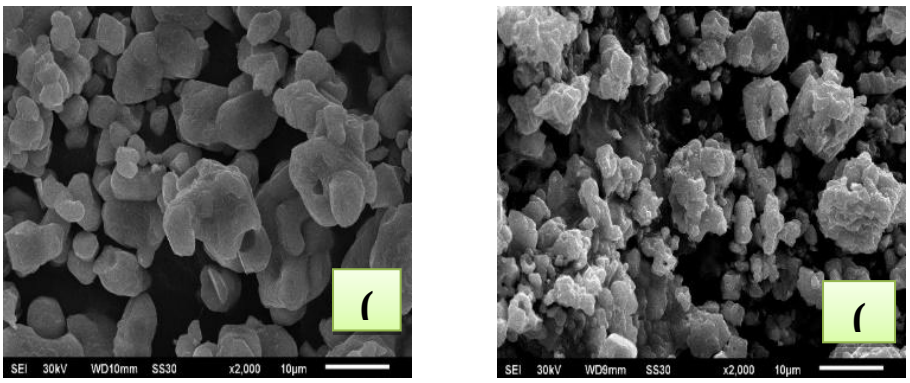

Fig. 8. SEM micrographs of $Mn_{1-x}Co_xMoO_4$ powders (a): x = 0.3 and (b): x = 0.6 prepared by sol-gel route.

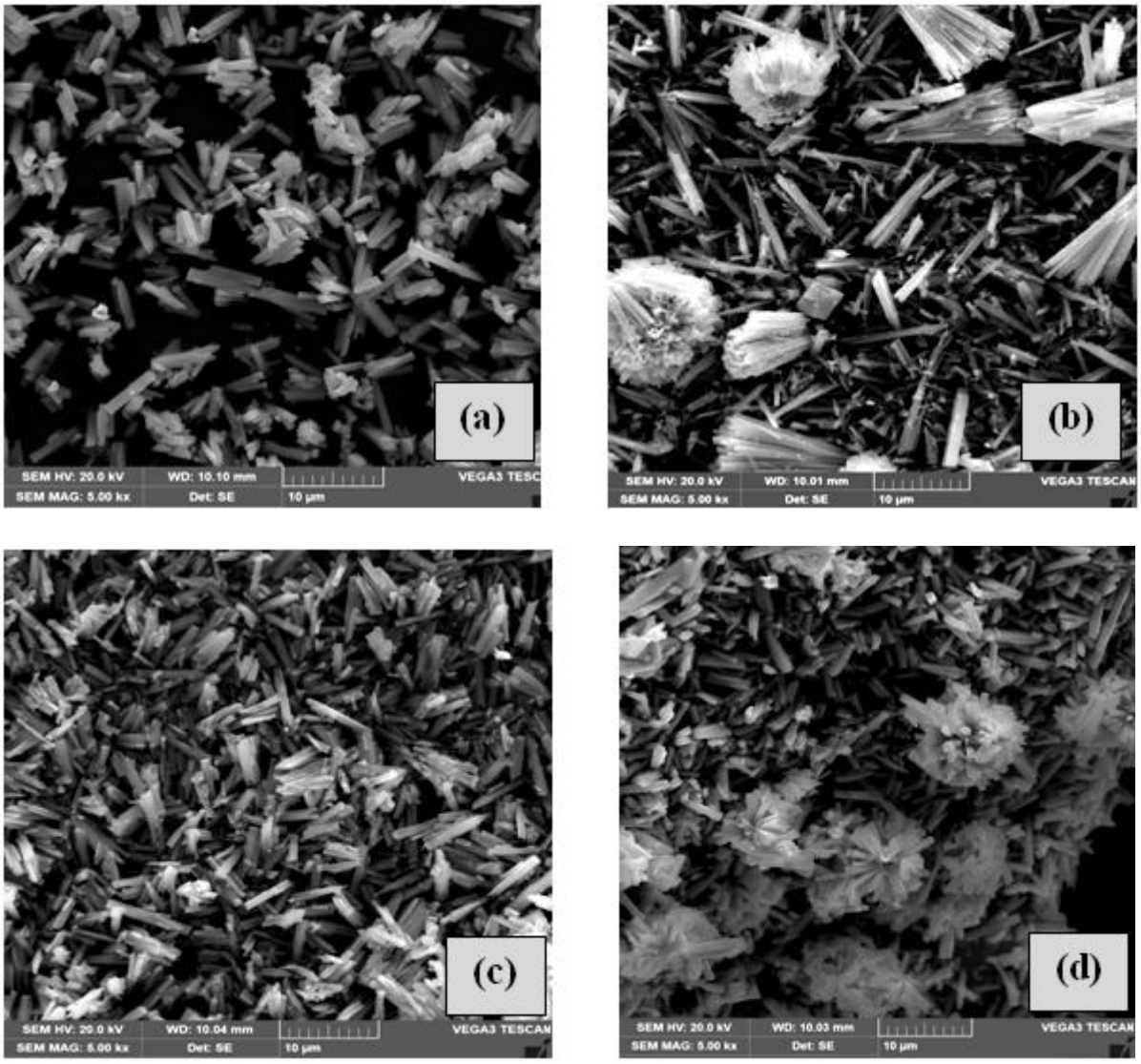

Fig. 9. SEM micrographs of $Mn_{1-x}Co_xMoO_4$ powders (a): x = 0, (b): x = 1, (c): x = 0.3 and (d): x = 0.6 prepared by co-precipitation.

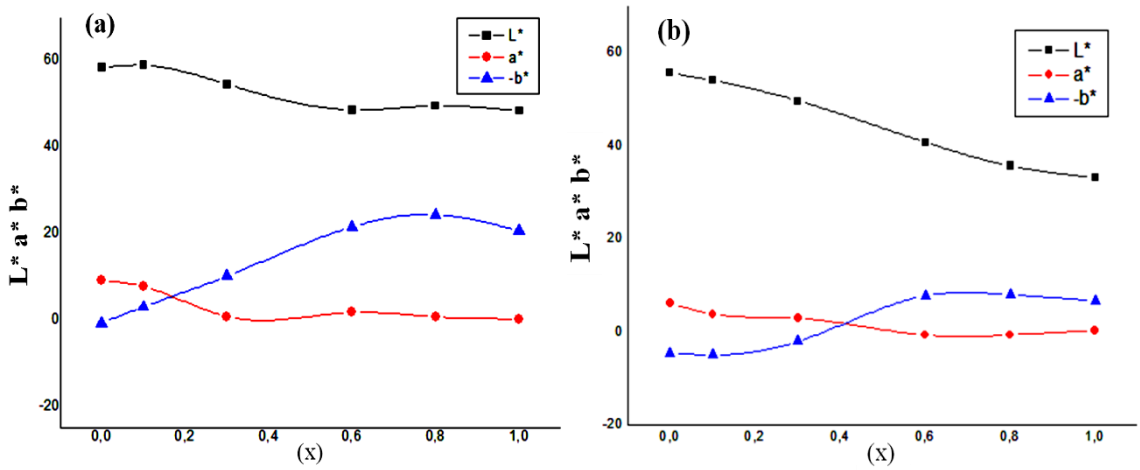

Fig. 10. Evolution of the color parameters of $Mn_{1-x}Co_xMoO_4$ ($0 \leq x \leq 1$) powders obtained by sol-gel route at 700°C **(a)** and by co-precipitation at 500°C **(b)** as a function of x.

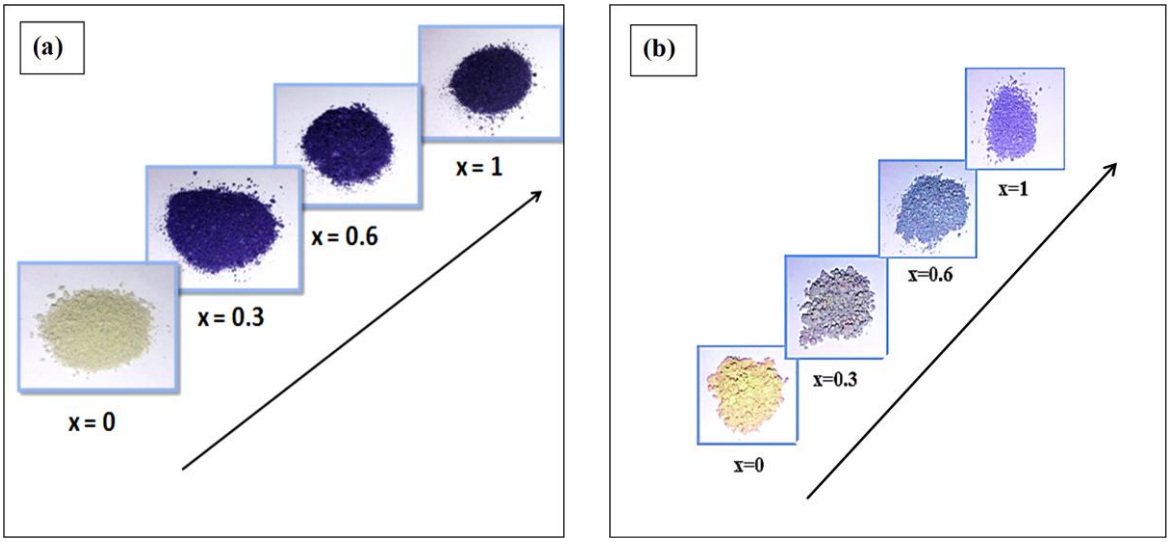

Fig.11. The colors of $Mn_{1-x}Co_xMoO_4$ ($0 \leq x \leq 1$) powders synthesized by sol-gel at 700°C **(a)** and by co-precipitation at 500°C **(b)**.

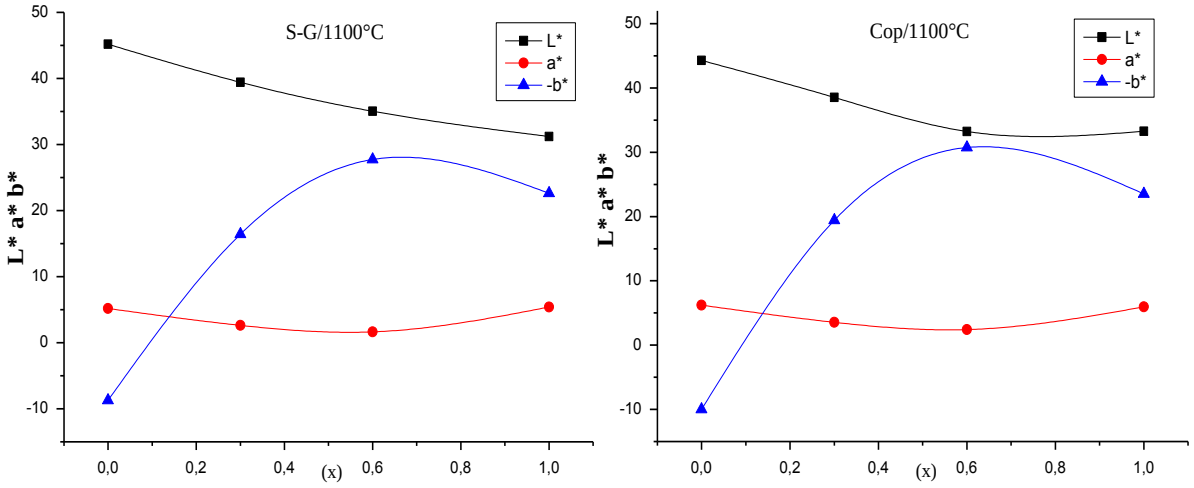

Fig. 12. Evolution of the color parameters of $Mn_{1-x}Co_xMoO_4$ ($0 \leq x \leq 1$) powders elaborated at 1100°C by sol-gel route **(S-G)** and by co-precipitation **(Cop)** as a function of x.

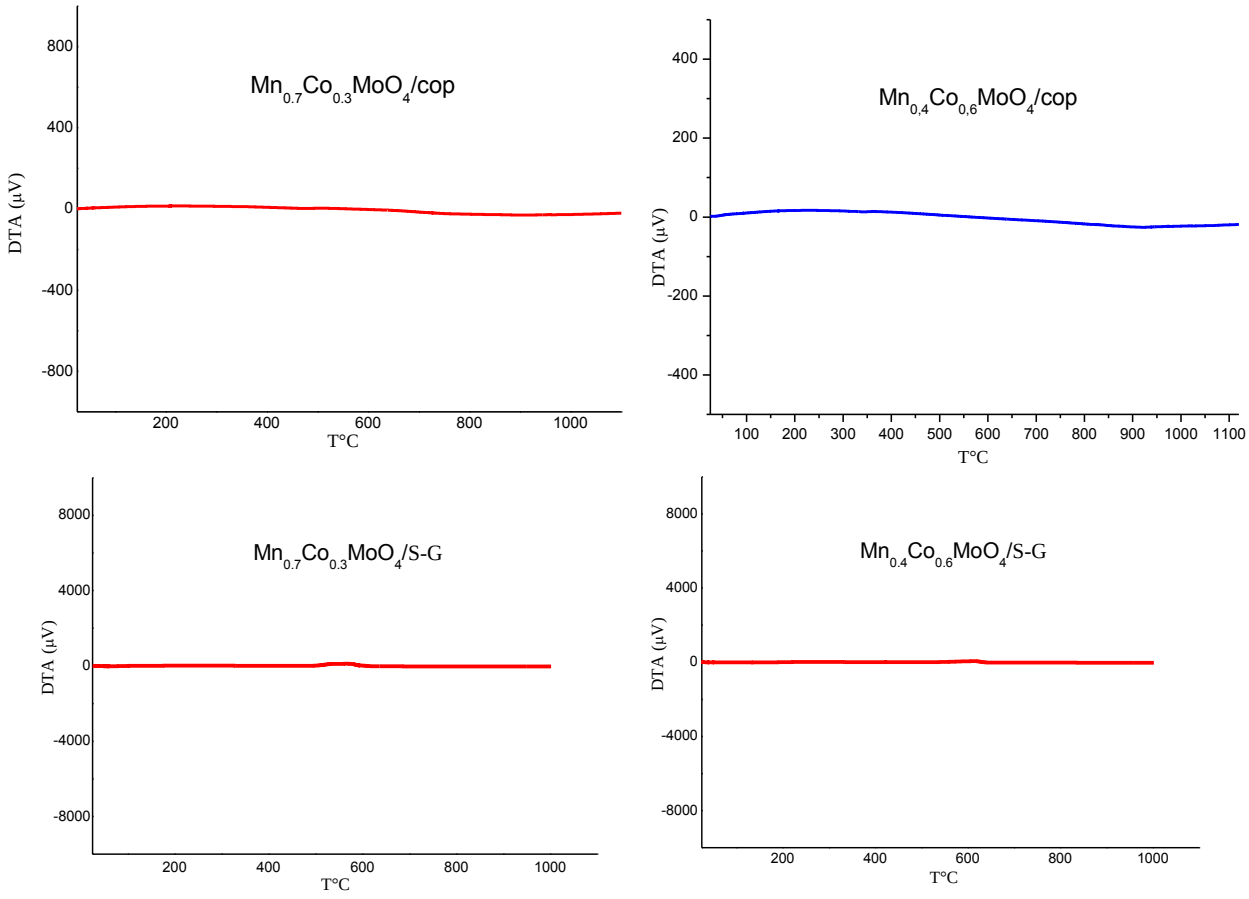

Fig.13. DTA analysis of $Mn_{0.7}Co_{0.3}MoO_4$ and $Mn_{0.4}Co_{0.6}MoO_4$ powders obtained by sol-gel route at 700°C **(S-G)** and by co-precipitation at 500°C **(Cop)**.

Table 1

Specific surface areas of $Mn_{0.7}Co_{0.3}MoO_4$ and $Mn_{0.4}Co_{0.6}MoO_4$ powders prepared by sol-gel and by co-precipitation.

Method of synthesis	Incorporation rate of Co^{2+}	Specific surface area BET (m^2/g)
Sol- gel	0.3	0.15
(700°C)	0.6	0.22
Co-precipitation	0.3	6.39
(500°C)	0.6	7.52

Table 2

Colorimetric coordinates of $Mn_{0.7}Co_{0.3}MoO_4$ and $Mn_{0.4}Co_{0.6}MoO_4$ powders measured before and after tests by chemical agents.

Sample		$Mn_{0.7}Co_{0.3}MoO_4$			$Mn_{0.4}Co_{0.6}MoO_4$		
Colorimetric coordinates		**L***	**a***	**b***	**L***	**a***	**b***
Before tests		54.48	0.83	-10.15	48.64	1.75	-21.69
After tests	HNO_3	54.46	0.81	-10.13	48.63	1.72	-21.67
10% Acid /Base	NaOH	54.47	0.82	-10.14	48.62	1.73	-21.68